Efficient Two-Photon Absorbing Acceptor-π-Acceptor Polymethine Dyes

**Lazaro A. Padilha,*,† Scott Webster,† Olga V. Przhonska,†,‡ Honghua Hu,† Davorin Peceli,†
Trenton R. Ensley,† Mykhailo V. Bondar,‡ Andriy O. Gerasov,§ Yuriy P. Kovtun,§
Mykola P. Shandura,§ Alexey D. Kachkovski,§ David J. Hagan,† and Eric W. Van Stryland†**

*CREOL, The College of Optics and Photonics, University of Central Florida, Orlando, Florida 32826, Institute
of Physics, National Academy of Sciences, Kiev, 03028, Ukraine, and Institute of Organic Chemistry, National
Academy of Sciences, Kiev, 03094, Ukraine*

We present an experimental and theoretical investigation of the linear and nonlinear optical properties of a series of acceptor-π-acceptor symmetrical anionic polymethine dyes with diethylamino-coumarin-dioxaborine terminal groups and different conjugation lengths. Two-photon absorption (2PA) cross sections (δ_{2PA}) are enhanced with an increase of π-conjugation length in the investigated series of dyes. 2PA spectra for all dyes consist of two well-separated bands. The first band, located within the telecommunications window, occurs upon two-photon excitation into the vibrational levels of the main $S_0 \rightarrow S_1$ transition, reaching a large δ_{2PA} = 2200 GM (1 GM = 1 × 10^{-50} cm^4 s/photon) at 1600 nm for the longest conjugated dye. The position of the second, and strongest, 2PA band for all anionic molecules corresponds to the second-excited final state, which is confirmed by quantum-chemical calculations and excitation anisotropy measurements. Large δ_{2PA} values up to 17 000 GM at 1100 nm are explained by the combination of the large ground- and excited-state transition dipole moments. The three shortest dyes show good photochemical stability and surprisingly large fluorescence quantum yields of ≈0.90, ≈0.66, and ≈0.18 at the red to near-IR region of ≈640, ≈730, and ≈840 nm, respectively. The excited-state absorption spectra for all samples are also studied and exhibit intense bands throughout the visible wavelength region with peak cross section close to 5 × 10^{-16} cm^2 with a corresponding red shift with increasing conjugation lengths.

Introduction

The search for new technologies based on nonlinear optical phenomena—such as optical telecommunications and switching, optical information processing, and bioimaging—has launched a growing interest in the development of novel nonlinear optical materials, including semiconductor quantum dots,[1] metal nano-structures,[2] and organic molecules.[3–6] In the field of organic molecules, significant experimental and theoretical studies have been devoted to design and understand molecules with optimized nonlinear optical properties and their structure−property relations. For many organic structures, including polymethine dyes, the primary sources of optical nonlinearity at the molecular level are the delocalized electrons in their π-conjugated systems.

More sophisticated molecular designs, based on the addition of electron-donor (D) and electron-acceptor (A) groups to the ends or the center of the π-conjugated backbone, have resulted in the development of more effective dipolar or quadrupolar-like structures: D-π-D (such as cationic symmetrical polyme-thines[7]), D-π-A-π-D (symmetrical polymethine-like squaraines or polyene-like tetraones for example[8]), A-π-A, A-π-D-π-A (such as symmetrical oxaborines[9–11] or fluorenes[12,13]), and asymmetrical D-π-A or push−pull molecules.[14–16] In previous studies, we have shown that the inclusion of a squaraine acceptor bridge into the D-π-D polymethine chromophore, resulting in a D-π-A-π-D structural motif, leads to an increase in the density of final states, drastically enhancing the two-photon absorption

(2PA) cross-section (δ_{2PA}).[8,17] Recent publications have shown that for "extended" squaraines, δ_{2PA} can exceed 30 000 GM (1 GM = 1 × 10^{-50} cm^4 s/photon) at the 2PA peak.[18] Anionic dioxaborine polymethines A-π-A, described in the literature, are characterized by large refractive third-order nonlinearities[10] in the near-IR wavelength range and relatively small $\delta_{2PA} \approx$ 500−700 GM.[9–11]

In the current work, we report very large 2PA cross sections (up to 17 000 GM) for a series of anionic symmetric A-π-A diethylamino-coumarin-dioxaborine polymethines with different conjugation lengths. Detailed experimental and quantum-chemical investigations of the linear and nonlinear optical absorption properties in this series of dyes are performed to explain the origin of large 2PA, which is comparable to previously studied symmetrical squaraines.[8,17,18] In this paper, we first describe the electronic structure of the symmetrical A-π-A molecules and their linear optical properties (absorption, fluorescence, quantum yield, and anisotropy). We then present the experimental methods used for determining lifetimes, 2PA, excited-state absorption (ESA) followed by the experimental results. Analyzing the 2PA and ESA spectra along with quantum-chemical calculations provides insights into their photophysical nature, in particular, the origin of the large 2PA cross sections.

2. Experimental Methods and Results

2.1. Materials Characterization and Linear Spectroscopic Properties. The molecular structures of the dyes studied in this paper are shown on the left of Figure 1a−d. Their chemical names are: tributylammonium 2,2-difluoro-4-[3-(8-(diethylamino)-2,2-difluoro-5-oxo-(5H)-chromeno[4,3-d]-1,3,2-(2H)-dioxaborin-4-ylidene)-1-propenyl]-5-oxo-(5H)-8-diethylamino)-chromeno[4,3-

* To whom correspondence should be addressed. E-mail: padilha@creol.ucf.edu.
† University of Central Florida.
‡ Institute of Physics, National Academy of Sciences.
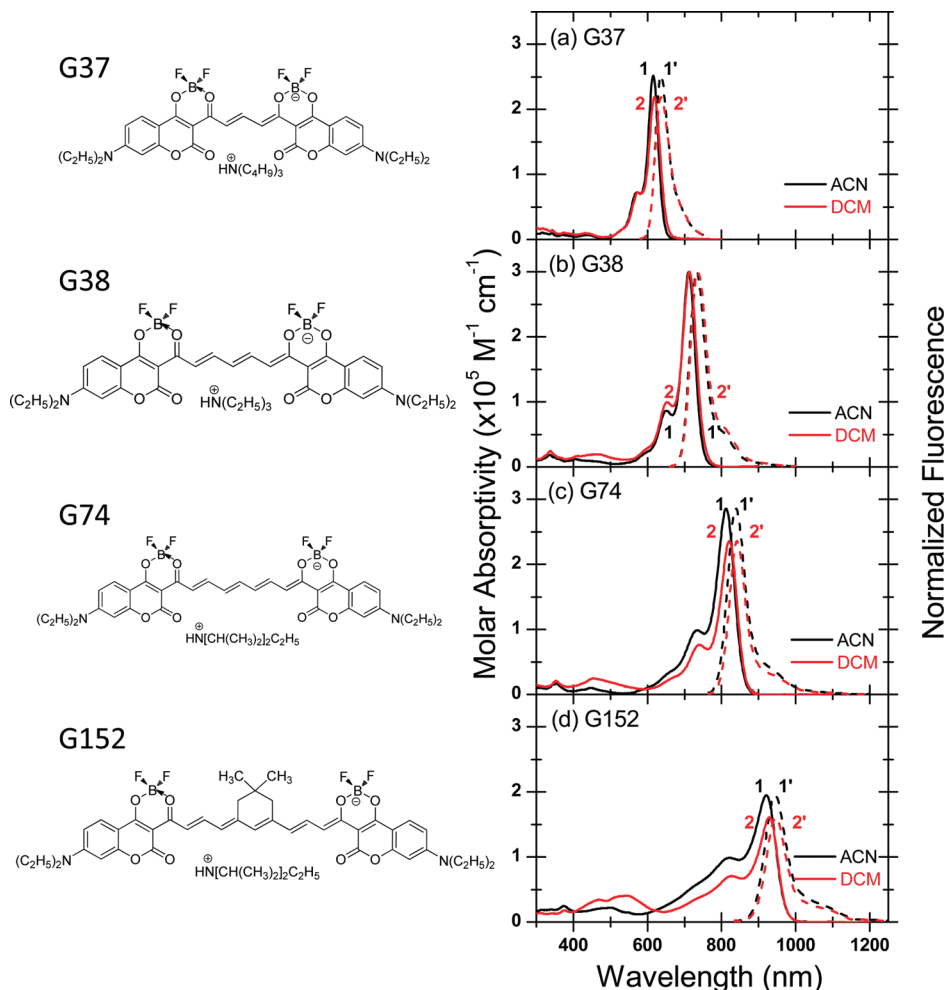§ Institute of Organic Chemistry, National Academy of Sciences.

Figure 1. (Left) Molecular structures of A-π-A polymethines studied. (Right) Molar absorptivities (not primed) and normalized fluorescence (primed) spectra in (1) DCM and (2) ACN of G37 (a), G38 (b), G74 (c), and G152 (d).
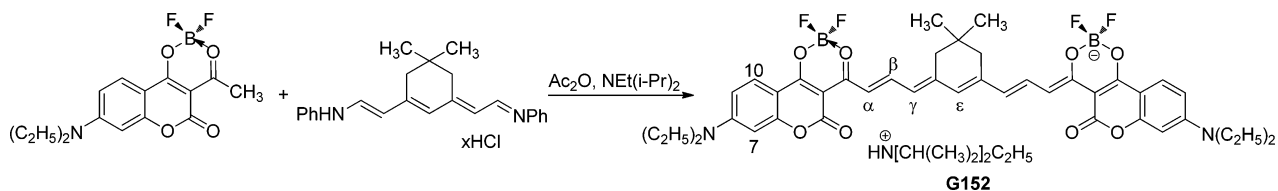

Figure 2. Synthetic schematic of G152.

d]-1,3,2-(2H)-dioxaborinate, labeled as G37; triethylammonium 2,2-difluoro-4-[5-(8-(diethylamino)-2,2-difluoro-5-oxo-(5H)-chromeno[4,3-d]-1,3,2-(2H)-dioxaborin-4-ylidene)-1,3-pentadienyl]-8-(diethylamino)-5-oxo-(5H)-chromeno[4,3-d]-1,3,2-(2H)-dioxaborinate, labeled as G38; diisopropylethylammonium 2,2-difluoro-4-[7-(2,2-difluoro-5-oxo-(5H)-8-(diethylamino)-chromeno[4,3-d]-1,3,2-(2H)-dioxaborin-4-ylidene)-1,3,5-heptatrienyl]-5-oxo-(5H)-8-(diethylamino)-chromeno[4,3-d]-1,3,2-(2H)-dioxaborinate, labeled as G74; and diisopropylethylammonium 2,2-difluoro-4-[4,6-(2,2-dimethyl)-trimethylen-9-(2,2-difluoro-5-oxo-(5H)-8-(diethylamino)-chromeno[4,3-d]-1,3,2-(2H)-dioxaborin-4-ylidene)-1,3,5,7-nonanotetraenyl]-5-oxo-(5H)-8-(diethylamino)-chromeno[4,3-d]-1,3,2-(2H)-dioxaborine, labeled as G152. All four dyes contain the same diethylamino-coumarin-dioxaborine acceptor terminal groups, possessing delocalized π-electron systems that may increase the overall π-conjugation, and differ by the lengths of their vinylene chain, n, from the shortest $n = 1$ in G37 to the longest $n = 4$ in G152. Dyes G37, G38, and G74 have an unsubstituted conjugated chain, whereas G152 includes a bridge unit in the

center of the chain, which is a known method to increase photo and chemical stability for long linearly conjugated absorbing molecules.[19] The synthesis of G37, G38, and G74 was recently described in ref 20. Synthesis of the new compound, G152, was performed following the schematic presented in Figure 2. [Yield 135 mg (32%). Mp 277−280 °C. ^{1}H NMR (DMSO-d_6) δ: 1.03 (s, 6 Í, C(CH$_3$)$_2$), 1.15−1.25 (m, 27 H, CH$_3$), 3.12 (m, 4 H, CH$_2$), 3.48 (m, 12 H, NCH$_2$), 6.45 (d, $^3J_{H,H}$ = 14.4 Hz, 2 H, γ-H), 6.51 (s, 3 H, 7-H, ε-H), 6.78 (d, $^3J_{H,H}$ = 9.0 Hz, 2 H, 9-H), 7.21 (d, $^3J_{H,H}$ = 12.9 Hz, 2 H, α-H), 7.69 (d, $^3J_{H,H}$ = 9.0 Hz, 2 H, 10-H), 7.87 (m, 2 H, β-H), 8.16 (br s, 1H, N$^+$H). Anal. Calcd. for C$_{50}$H$_{63}$B$_2$F$_4$N$_3$O$_8$: C, 64.45; H, 6.77; N, 4.51. Found: C, 64.27; H, 6.69; N, 4.53.] A mixture of 2,2-difluoro-4-methyl-5-oxo-(5H)-8-(diethylamino)-chromeno[4,3-d]-1,3,2-(2H)-dioxaborine (292 mg, 0.9 mmol) and 3,5-[(2,2-dimethyl)-trimethylen]-1,7-di(phenylamino)-1,3,5-heptatrien hydrochloride (171 mg, 0.45 mmol) in acetic anhydride (1.5 mL) was refluxed for 1−2 min. The solvent was removed under vacuum. Acetonitrile (0.5 mL) and diisopropylethylamine (0.5 mL) were added and the resulting mixture was stirred at room temperature

Efficient Two-Photon Absorbing Polymethine Dyes

J. Phys. Chem. A, Vol. 114, No. 23, 2010 **6495**

TABLE 1: Spectroscopic Parameters of G37, G38, G74, and G152 in ACN and DCM[a]

dye (solvent)	λ_{Abs}^{max} (nm)	λ_{Fl}^{max} (nm)	ε^{max} ($\times 10^5$ $M^{-1}cm^{-1}$)	η	τ_F calculated from eq 1 (ns)	τ_F picosecond pump–probe (ns)	μ_{01} transition dipole moment ($S_0 - S_1$) (Debye)
G37 (DCM)	618	637	2.19	0.89 ± 0.05	2.2 ± 0.2		14
G37 (ACN)	615	636	2.52	0.86 ± 0.05	2.3 ± 0.2	1.8 ± 0.3	14
G38 (DCM)	713	735	3.00	0.57 ± 0.03	1.4 ± 0.2		17
G38 (ACN)	711	733	3.00	0.66 ± 0.03	2.0 ± 0.2	1.8 ± 0.3	16
G74 (DCM)	820	842	2.36	0.17 ± 0.02	0.75 ± 0.15		16
G74 (ACN)	812	839	2.86	0.18 ± 0.02	0.65 ± 0.13	0.7 ± 0.1	18
G152 (DCM)	928	947	1.61	0.02 ± 0.01	0.15 ± 0.07		16
G152 (ACN)	921	945	1.95	0.02 ± 0.01	0.12 ± 0.06	0.12 ± 0.02	20

[a] λ_{Abs}^{max} and λ_{Fl}^{max} are the peak absorption and fluorescence wavelengths; ε^{max} is the peak extinction coefficients; η and τ_F are the fluorescence quantum yields and lifetimes; and μ_{01} are the transition dipole moments, respectively.

for 12 h. The precipitate was filtered off and washed with acetonitrile (ACN).

The linear absorption spectra of all molecules, recorded by a Varian Cary 500 spectrophotometer, are presented in Figure 1a−d with the most significant linear properties listed in Table 1. Absorption spectra were measured in two solvents with different polarity: spectroscopic grade dichloromethane (DCM) and ACN. Solvents with polarities less than that of DCM could not be used due to the low solubility. The absorption spectra for this current series of dyes are composed of intense cyanine-like bands, attributed to their $S_0 \rightarrow S_1$ transitions, with the main absorption peaks shifting by $\approx$100 nm to longer wavelengths with the lengthening of the main conjugation chain, and a relatively weak linear absorption in the visible and ultraviolet regions corresponding to absorption to higher excited-states, $S_0 \rightarrow S_n$ transitions. Increasing solvent polarity from DCM to ACN leads to a small hypsochromic shift (3−7 nm) of the main absorption peak, which may be attributed to stabilization of the ground state in ACN. All dyes are more photochemically stable in ACN than in DCM, determined by an increasing absorption band appearing at ∼500 nm after several hours in DCM, presumed to be a photoproduct from decomposition. Additionally, note that both solvents lead to a substantial band broadening for G152, evidenced by an increase of the vibrational shoulder of the main transition, which is stronger in the more polar solvent ACN. This effect is connected with ground-state symmetry breaking, described previously for symmetrical cationic polymethines.[21]

The fluorescence spectra of all compounds in DCM and ACN, measured by a PTI QuantaMaster spectrofluorimeter equipped with a nitrogen-cooled (77 K) Hamamatsu R5509−73 photomultiplier tube detector, are shown in Figure 1a−d. All fluorescence spectra are corrected for the spectral responsivity of the detection system. In contrast to absorption, fluorescence spectra for all dyes are narrow and appear to be independent of solvent polarity. Fluorescence quantum yields, η, are measured using the standard method of comparison for G37 and G38 with a known "red" standard dye, Cresyl Violet perchlorate (CAS No. 41830−80−2, Sigma Aldrich) in methanol, which has an absorption peak at 594 nm, fluorescence peak at 620 nm, and a fluorescence quantum yield, η, of 0.54 ± 0.03.[22] The fluorescence quantum yield for G74 and G152 is measured by comparison with our previously proposed standard for the near-IR wavelength range, dye PD 2631 in ethanol, with an absorption peak at 784 nm, fluorescence peak at 809 nm, and $\eta = 0.11 \pm 0.01$.[23] Our experiments show that the polarity of the solvents does not significantly affect the positions of absorption and fluorescence spectra and the values of the fluorescence quantum yields. Note that all investigated dyes, especially G37 and G38, are highly fluorescent molecules with

quantum yields of 0.90 ± 0.05 and 0.66 ± 0.03 respectively, as shown in Table 1. To our knowledge, these values are among the largest fluorescence quantum yields in the near-IR range, which is desirable for different fluorescence sensing applications. From spectroscopic measurements, we estimate the fluorescence lifetime, $\tau_F = \eta\tau_R$, where the natural lifetime, τ_R, can be calculated from the Strickler−Berg equation:[25]

$$1/\tau_R = 2.88 \times 10^{-9} n^2 \varepsilon^{max} \left[\frac{\int F(\nu)d\nu \times \int \frac{\varepsilon(\nu)}{\nu}d\nu}{\int \frac{F(\nu)}{\nu^3}d\nu} \right]$$

(1)

where $F(\nu)$ and $\varepsilon(\nu)$ are the normalized fluorescence and absorption spectra, and ε^{max} is the extinction coefficient at the peak absorption. The fluorescence lifetimes, estimated and measured by a picosecond degenerate pump−probe technique in ACN (see Section 2), are shown in Table 1, and both agree to within 20%.

With one-photon excitation anisotropy measurements,[24] we can determine the spectral positions of the optical transitions and the orientation of the transition dipole moments. These fluorescence anisotropy measurements are performed using viscous solutions of ethylene glycol (more viscous solvents could not be used due to the low solubility of the dyes) to reduce rotational reorientation and at low concentrations (C $\approx$ 10^{-6} M) to avoid reabsorption of the fluorescence. The anisotropy, calculated as $r(\lambda) = [I_{\parallel}(\lambda) - I_{\perp}(\lambda)]/[I_{\parallel}(\lambda) + 2I_{\perp}(\lambda)]$, is measured by observing the emission wavelength, typically near the fluorescence maximum, with a fixed polarization. Then, the fluorescence intensity is recorded as a function of excitation wavelength λ at polarizations parallel ($I_{\parallel}(\lambda)$) and perpendicular ($I_{\perp}(\lambda)$) to the emission polarization. As shown in Figure 3a−d, the excitation anisotropy spectra reveal large alternations of peak and valley features for all molecules. Analysis of the anisotropy spectra, linked to quantum-chemical calculations, allows us to locate the positions of one-photon forbidden transitions, such as transitions between states of the same symmetry, and therefore, possible transition energies of the final electronic states in the 2PA spectra. We have previously, successfully applied this method to study the 2PA properties in series of both symmetrical cationic D-π-D[7] and asymmetrical D-π-A[26] dyes. As shown in Figure 3a−d, the excitation anisotropy function $r(\lambda)$ is constant ($r \approx 0.35$) in the broad spectral range 500−650 nm for G37, 540−730 nm for G38, 560−800 nm for G74, and 620−900 nm for G152, indicating a nearly parallel orientation of the absorption $S_0 \rightarrow S_1$ and the $S_1 \rightarrow S_0$ emission transition dipole moments. In the shorter wavelength region, the anisotropy
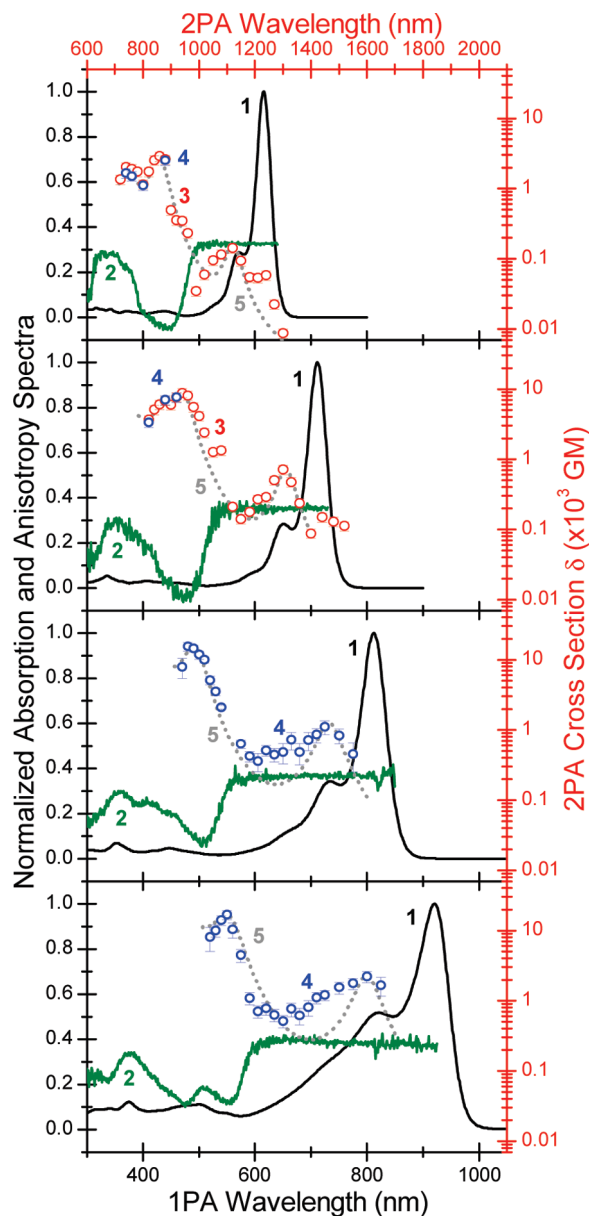
Figure 3. Normalized one-photon absorption (1), excitation anisotropy (2), and two-photon absorption spectra for G37 (a), G38 (b), G74 (c) and G152 (d) in ACN. Two-photon absorption spectra experimentally obtained by two-photon fluorescence (3), by single wavelength Z-scan (4), and fitting with eq 4 (dotted line 5) are shown on the right and top axis.

spectrum for G37 shows a broad minimum at ≈390−460 nm ($r \approx -0.05$), followed by a broad peak at ≈320−370 nm (with the shoulder around 370 nm), and the next decrease at ≈290 nm. The anisotropy spectrum for G38 exhibits similar structures with narrower minimum at ≈440−480 nm, peak at ≈350 nm, and then a decrease at ≈300 nm. Anisotropy minima for both dyes indicate the position of one-photon forbidden transitions $S_0 \rightarrow S_n$ forming ≈50−60° angles with the emission dipole moment. An increase in the conjugation lengths from G37 to G152 demonstrates the evolution of the excitation anisotropy spectra: for G74 an anisotropy minimum at ≈500 nm becomes sharper and narrower with the value $r \approx 0.05$, and for G152 this minimum is clearly separated into two structures with increased anisotropy values $r \approx 0.1$ at ≈550 and ≈470 nm. On the basis of quantum-chemical calculations (see Section 4), we conclude that the broad minima in the excitation anisotropy spectra correspond to the overlapping of several transitions that

become more separated for the dyes G74 and especially G152 with the longer conjugated chain. Values for the $S_0 \rightarrow S_1$ transition dipole moments $\boldsymbol{\mu}_{01}$ for all molecules are calculated from the integrated area of the main absorption band $S_0 \rightarrow S_1$, $\mu_{01} = \{[1500(\hbar c)^2 \ln 10] \int \varepsilon_{01}(\nu) d\nu / \pi N_A E_{01}\}^{1/2}$, where $\varepsilon_{01}(\nu)$ is the extinction coefficient, N_A is Avogadro's number, and E_{01} is the peak energy of the main transition.[24] Calculations indicate that all dyes have similar and relatively large transition dipole moments, when compared to other single organic molecules, $\mu_{01} = 13$ D − 20 D as shown in Table 1.

2.2. Nonlinear Characterization Methods and Results. The linear optical characterization has shown that there are no significant changes in the optical properties for different solvent polarity, see Table 1. Therefore, nonlinear spectral measurements were performed in the polar solvent ACN due to the higher solubility and photostability of the investigated dyes in this solvent. Tunable laser systems with femtosecond (for 2PA and ESA spectra) and picosecond (for ESA dynamics) pulsewidths are used for the nonlinear optical characterization. The picosecond measurements are performed with a 10 Hz modelocked Nd:YAG laser (EKSPLA, model PL2143) operating at 1064 nm and doubled to 532 nm, with a pulsewidth of 15 ps (FWHM), measured by second harmonic autocorrelation. The femtosecond measurements are performed using two optical parametric generator/amplifiers (OPG/OPA Light Conversion Ltd., model TOPAS-800), which can be independently tuned from 300 nm to 2.6 μm, with pulsewidths 100−140 fs (FWHM) measured by autocorrelation techniques. Both OPG/OPAs are pumped by a Clark-MXR Ti:Sapphire regenerative amplifier, CPA-2010, delivering ~2 mJ pulses at 775 nm and 140 fs (FWHM) pulsewidth at a 1 kHz repetition rate.

The ESA spectra are measured using the femtosecond pump and white-light continuum (WLC) probe as described in ref 27. The pump is set at the peak of the linear absorption for each molecule and the probe is selected from a WLC using narrow band spectral filters of ≈10 nm in order to improve the signal-to-noise ratio and to avoid stimulated emission.[28] Using the values of $\sigma_{1n}(\lambda_{ESA})$, measured independently by picosecond Z-scans[29] at $\lambda_{ESA} = 532$ nm, the absolute values for $\sigma_{1n}(\lambda)$ and N_1 are obtained for each molecule from eq 2:[21]

$$\sigma_{1n}(\lambda) = \sigma_{01}(\lambda) - (\sigma_{01}(\lambda_{ESA}) - \sigma_{1n}(\lambda_{ESA})) \times \frac{\ln(^{T_{NL}}/_{T_L}|_{\lambda})}{\ln(^{T_{NL}}/_{T_L}|_{\lambda_{ESA}})} \quad (2)$$

The nonlinear refractive index of neat carbon disulfide (CS$_2$) via closed-aperture Z-scan[29] is used to verify the alignment of the picosecond Z-scan setup and to determine the focused beam spot size. Z-scan measurements were performed at 532 nm, using several input energies and fit with a three-level singlet model using the rate and propagation eqs 3:

$$\frac{dI}{dz} = -\sigma_{01}N_0 I - \sigma_{1n}N_1 I$$
$$\frac{dN_0}{dt} = -\frac{\sigma_{01}N_0 I}{\hbar\omega} + \frac{N_1}{\tau_F}$$
$$\frac{dN_1}{dt} = \frac{\sigma_{01}N_0 I}{\hbar\omega} - \frac{N_1}{\tau_F} - \frac{\sigma_{1n}N_1 I}{\hbar\omega} + \frac{N_n}{\tau_{n1}} \quad (3)$$
$$\frac{dN_n}{dt} = \frac{\sigma_{1n}N_1 I}{\hbar\omega} - \frac{N_n}{\tau_{n1}}$$

Efficient Two-Photon Absorbing Polymethine Dyes

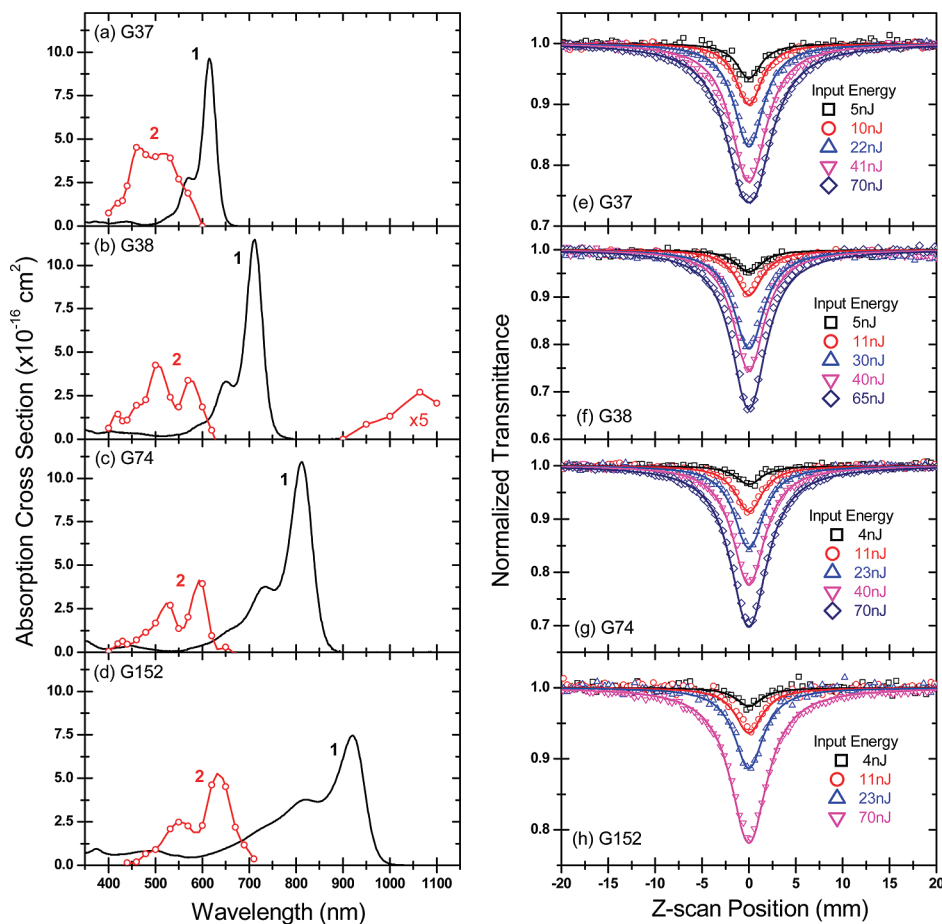*J. Phys. Chem. A, Vol. 114, No. 23, 2010* **6497**

Figure 4. (Left) One-photon and excited-state absorption spectra for G37 (a), G38 (b), G74 (c), and G152 (d) in ACN. (Right) Picosecond open-aperture Z-scan measurements for G37 (e), G38 (f), G74 (g), and G152 (h) in ACN.

where $N = N_0 + N_1 + N_n$, and τ_{n1} is the nonradiative decay from state S_n to S_1, and τ_F is the experimentally measured fluorescence lifetime. Figure 4a−d shows the ESA spectra measured for samples G37, G38, G74, and G152 in ACN.

Estimation of fluorescence lifetimes performed from the steady state measurements indicated that the investigated compounds are characterized by lifetimes ranging from 120 ps to 2.3 ns; hence, the use of a picosecond pump−probe technique is appropriate for the direct measurement of τ_F. In picosecond pump−probe measurements, a strong linearly polarized pump pulse excites the molecules and creates a population distribution in the excited-state that can be monitored as a function of time by a less intense probe pulse. In our experiments, both pump and probe beams at 532 nm were focused to spot sizes of ≈ 70 and ≈ 35 μm (HW1/e^2 M), respectively. The probe beam can be delayed up to 15 ns, and its fluence was kept much smaller than that of the pump (probe approximately 0.1% of the pump fluence) to avoid probe nonlinearities. Pump and probe beams were overlapped at a small angle $\approx 5°$ within the sample and with the probe beam polarized at the "magic" angle (54.7°) with respect to the pump in order to avoid contributions from reorientation effects.[30] Under these conditions, the probe decay is completely independent of polarization anisotropy, is monoexponential, and corresponds to the lifetime τ_F. The results are presented in Table 1.

The only free parameters used for the fittings of Z-scans are σ_{1n} and τ_{n1}. τ_{n1} only becomes important for large changes in transmittance where significant population in the upper excited-state usually occurs, so that σ_{1n} may be fit independently using small transmittance-change data. For each sample, the fitting

for all energies is done using the same set of parameters. From these results it is found: for G37, the ESA spectrum is broad and slightly divided into two bands with $\sigma_{1n}(460 \text{ nm}) = 4.5 \times 10^{-16}$ cm^2 and $\sigma_{1n}(530 \text{ nm}) = 3.9 \times 10^{-16}$ cm^2; for G38, the ESA spectrum consists of two more separated bands with $\sigma_{1n}(500 \text{ nm}) = 4.2 \times 10^{-16}$ cm^2 and $\sigma_{1n}(570 \text{ nm}) = 3.4 \times 10^{-16}$ cm^2; for G74, the ESA bands are shifted into the red region at ≈ 30 nm with $\sigma_{1n}(530 \text{ nm}) = 2.7 \times 10^{-16}$ cm^2 and $\sigma_{1n}(600 \text{ nm}) = 3.9 \times 10^{-16}$ cm^2 (note that the second band becomes more intense); and the same trend is observed for ESA bands for G152 with $\sigma_{1n}(550 \text{ nm}) = 2.5 \times 10^{-16}$ cm^2 and $\sigma_{1n}(620 \text{ nm}) = 4.6 \times 10^{-16}$ cm^2. The error bars are $\pm 15\%$ for the ESA maximum values. Further discussion of ESA is found in Section 3.2.

The degenerate 2PA spectrum is measured for all dyes in ACN using two experimental methods, two-photon excited fluorescence (2PF) and single wavelength open-aperture Z-scan, both with femtosecond excitation. The 2PF technique is more sensitive for measuring samples with relatively large fluorescence quantum yields (>1%) and can be applied to dyes with fluorescence peaks at wavelengths shorter than 800 nm (due to limitations of our fluorescence detection system). The 2PF experiment is performed using the tunable femtosecond source as described in ref 31. For each wavelength measured, the 2PA cross-section is calculated based on the results for Rhodamine B in methanol.[31] The quadratic dependence of the fluorescence on the pump irradiance is also verified to avoid any possible influence of one-photon excited fluorescence (1PF) on the results. At 2PA wavelengths close to the edge of the linear absorption, scattered pump, and/or 1PF can lead to inaccurate and erroneous results, so the results have to be double-checked

TABLE 2: Linear and Nonlinear Absorption Parameters of G37, G38, G74, and G152 in ACN[a]

dye (solvent)	1PA		ESA		2PA	
	λ_{Abs}^{max} (nm)	σ_{01}^{max} ($\times 10^{-16}$ cm^2)	λ^{max} (nm)	σ_{1n}^{max} ($\times 10^{-16}$ cm^2)	λ^{max} (nm)	δ^{max} (GM)
G37 (ACN)	615	9.6	460	4.5 ± 0.7	860	2900 ± 500
G38 (ACN)	711	11.5	500	4.2 ± 0.6	940	8800 ± 1300
G74 (ACN)	812	10.9	600	3.9 ± 0.6	960	15000 ± 2300
G152 (ACN)	921	7.5	620	4.6 ± 0.7	1100	17000 ± 2500

[a] 1PA, λ_{Abs}^{max}, and σ_{01}^{max} are the peak ground-state absorption wavelengths and cross sections; ESA, λ^{max}, and σ_{1n}^{max} are the peak excited-state absorption wavelengths and cross sections; and 2PA, λ^{max} and δ^{max} are the peak two-photon absorption wavelengths and cross sections, respectively.

by open-aperture Z-scan. However, linear absorption can lead to excited-state absorption that can be indistinguishable from the 2PA in the open-aperture Z-scan results. In order to distinguish the instantaneous 2PA from the noninstantaneous ESA, time-resolved experiments are necessary.[8]

For dye G38, a significant portion of the fluorescence spectrum is longer than 800 nm and is beyond the calibrated detection limit of our 2PF system, so it is not possible to obtain the absolute values of the 2PA cross-section via 2PF. For this case, only the relative spectrum is obtained by 2PF and open-aperture Z-scan is performed to measure the absolute value of the cross sections. Excellent agreement for the 2PA spectrum and δ_{2PA} values for G37 (and other similar dyes as shown in ref 26) measured by both experiments, indicate that scaling of 2PF by the Z-scan technique is reasonable and accurate, contrary to other reports.[5,32] For every wavelength, the femtosecond Z-scan setup is aligned and calibrated by measuring the 2PA and nonlinear refractive index of semiconductors, ZnSe (for λ < 900 nm) and CdTe (for λ > 900 nm), and the nonlinear refractive index of CS$_2$. The fluorescence spectra for G74 and G152 lie beyond the detection limit of our 2PF system, therefore only open-aperture Z-scan was used for determination of their 2PA spectra. The results are shown in Figure 3a–d and are discussed in Section 3.2. The main nonlinear parameters measured for G37, G38, G74, and G152 in ACN are summarized in Table 2.

3. Discussion

3.1. Quantum-Chemical Approach. Quantum-chemical orbital analysis is performed with the goal of understanding the nature of 2PA and ESA spectra and revealing the origins of the large 2PA cross sections. Geometry optimization, energies of the molecular orbitals (MOs), and energies and oscillator strengths of electronic transitions are calculated in the framework of the standard semiempirical AM1 Hamiltonian (HyperChem Package). The typically applied ZINDO/S method cannot be used for the molecules under investigation due to the lack of parametrization for the boron (B) atom. The wave functions of the excited-states were built with the single configuration interaction technique taking into account 6 occupied and 3 unoccupied MOs (a total of 18 configurations). We have additionally verified that this number of configurations is sufficient to model the one- and two-photon absorption properties of the molecules studied in the near-ultraviolet, visible, and, near-IR ranges that are covered by the experimentally measured one- and two-photon absorption spectra. Also, the ordering of the MOs was checked by an ab initio method (6-31G** basis). All calculations are performed for the isolated molecules in vacuum, which is reasonable for symmetrical A-π-A compounds, which are almost insensitive to the solvent polarity. More detailed description of our quantum-chemical approach applied for this anionic series can be found in ref 33. This

methodology is a useful tool for understanding the nature of the orbitals and the transitions between them, including calculations of peak positions of 2PA and ESA. It has been applied previously to obtain a detailed understanding of the linear and nonlinear absorption properties in a series of polymethine, squaraine, and tetraone dyes.[8] Our calculations consider only the single-excitation configuration-interaction scheme since our primary goal is to reproduce the linear absorption spectra of the investigated molecules. With the linear absorption calculated, a symmetry analysis is performed to predict possible 2PA transitions by identifying one-photon allowed and forbidden transitions and to explain their nature. It should be noted that for some organic chromophores, higher order configuration-interaction schemes may give more accurate results for 2PA energies and cross sections. However for cyanine-like molecules, our previous experimental results and theoretical predictions for a variety of linear and nonlinear optical properties are in good agreement and have provided us with confidence that a single-excitation approach can be used instead of a more computationally expensive evaluation of double-excitation configuration-interaction scheme. Our previous results in conjunction with the current extensive experimental data allowed us to conclude that valuable insights may be gained by use of our quantum-chemical approach. The shapes of MOs for G37 are shown in Figure 5. This shows that the highest occupied molecular orbital (HOMO) represents a specific orbital (so-called solitonic level) with charge distributed within the chain only, mirror reflection of the cationic polymethines, whose solitonic level corresponds to the lowest unoccupied molecular orbital (LUMO).[8] HOMO−3 is a delocalized orbital, whereas HOMO−4 and HOMO−5 represent orbitals with the charge localized exclusively at the terminal groups. The main absorption band S$_0$ → S$_1$ corresponds to almost "pure" intense transitions from HOMO to LUMO; higher excited S$_0$ → S$_n$ transitions are mixed. Two predicted transitions, S$_0$ → S$_1$ and S$_0$ → S$_2$, are separated by a relatively large energy interval $\approx$0.7 eV; the experimental position of the S$_0$ → S$_2$ transition corresponds to a minimum in the excitation anisotropy spectrum and agrees with the calculated value. Several following transitions are strongly overlapped; their oscillator strengths are similar due to the contribution of the conjugated system from the terminal groups, which leads to a broad anisotropy valley as is seen in Figure 3a.

3.2. 2PA and ESA Spectra. Description and Analysis. Experimental 1PA and degenerate 2PA spectra for the anionic series in ACN are presented in Figure 3a–d with separate axes for 1PA (bottom) and 2PA (top) wavelengths. As shown in Figure 3a, the 2PA spectrum for G37 presents two well-separated bands: first band with $\delta_{2PA} \approx$ 2900 GM at 860 nm (2PA scale), and second 2PA band at an energy shifted to the "blue" range at $\approx$1000−1200 cm^{-1} from the peak of the S$_0$ → S$_1$ transition. This relatively small 2PA band with $\delta_{2PA} \approx$ 140 GM is typical for all symmetrical cyanine-like molecules and
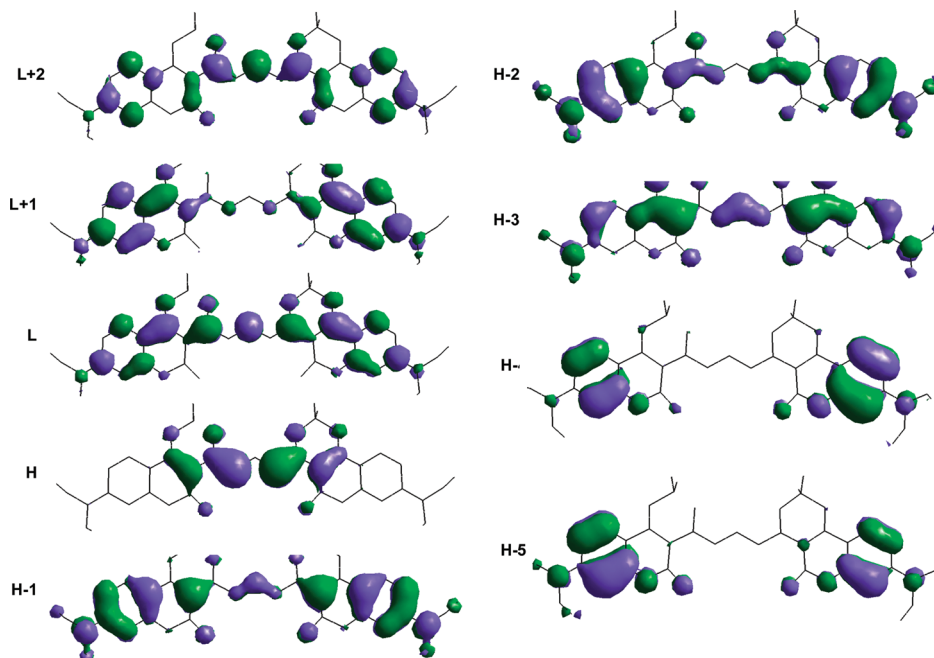
Figure 5. Molecular orbitals for G37 calculated in the framework of the standard semiempirical AM1 Hamiltonian (HyperChem Package).

can be attributed to the vibrational coupling between the first excited electronic state S_1 and its vibrational modes.[7,8,34] It is important to point out that the most intense 2PA band corresponds to the two-photon excitation into the S_2 state as follows from our quantum-chemical calculations. The position of the $S_0 \rightarrow S_2$ transition matches the minimum in excitation anisotropy spectrum (Figure 3a). The peak of the third 2PA band at a two-photon excitation of 740 nm with $\delta_{2PA} \approx 2000$ GM for G37 presumably corresponds to the mixture of $S_0 \rightarrow S_4$ and $S_0 \rightarrow S_6$ transitions and matches a small shoulder in the excitation anisotropy curve. A detailed quantum-chemical analysis allows us to examine the nature of 2PA bands for all these anionic dyes. Our calculations show that there are no additional electronic transitions in the spectral range of the lowest 2PA bands for all dyes, confirming their vibrational-assisted nature.[34,35] These 2PA bands are shifted to longer wavelengths, corresponding to the shift of the main peak with the lengthening of the conjugation chain, and their cross sections strongly increase: $\delta_{2PA} \approx 140$ GM at $\lambda_{2PA} = 1120$ nm for G37 ($n = 1$), $\delta_{2PA} \approx 710$ GM at $\lambda_{2PA} = 1300$ nm for G38 ($n = 2$), $\delta_{2PA} \approx 1100$ GM at $\lambda_{2PA} = 1450$ nm for G74 ($n = 3$), and $\delta_{2PA} \approx 2200$ GM at $\lambda_{2PA} = 1600$ nm for G152 ($n = 4$). The last value, $\delta_{2PA} \approx 2200$ GM, is one of the largest values for the single (not oligomeric or polymeric) organic molecules at the telecommunication wavelength range of 1300–1600 nm.[36,37] The origin of this large δ_{2PA} is probably connected with the large $\mu_{01} = 20$ D for G152 in ACN and a symmetry breaking effect.[7]

The strongest 2PA band for all dyes corresponds to the S_2 final state, which is confirmed by quantum-chemical calculations and excitation anisotropy measurements. Similar to the first 2PA band, δ_{2PA} for the second 2PA band increases with lengthening of the chain: $\delta_{2PA} \approx 2900$ GM at $\lambda_{2PA} = 860$ nm for G37, $\delta_{2PA} \approx 8800$ at $\lambda_{2PA} = 940$ nm for G38, $\delta_{2PA} \approx 15\,000$ GM at $\lambda_{2PA} = 960$ nm for G74, and $\delta_{2PA} \approx 17\,000$ GM at $\lambda_{2PA} = 1100$ nm for G152. The third 2PA band, observed in G37, becomes less separated from the second 2PA band for G38 ($\delta_{2PA} \approx 6800$ GM at $\lambda_{2PA} = 880$ nm). For G74 and G152 this band cannot be reached due to the influence of the linear absorption edge. Figure 3a–d clearly demonstrates that for the linear cyanine-like

molecules, the experimentally simple linear excitation anisotropy method can offer insights to predict the peak positions of 2PA bands.

To understand the origin of large δ_{2PA} (up to $\approx 17\,000$ GM) for diethylamino-coumarin-dioxaborine dyes, we reproduced the shapes of 2PA spectra for all dyes by using the experimental and calculated molecular parameters, and performed molecular modeling as follows: initial S_0 level, intermediate S_1 state, and two or three final states fi, depending on the number of experimentally observed 2PA bands. Fitting is presented in Figure 3 for all dyes in this study. For dye G37, the final states are: $f1$ (corresponding to vibrational levels of S_1), $f2$ (corresponding to the S_2 state), and $f3$ (involving the S_4 and S_6 states). In the approximation that all dipole moments μ_{1fi} are parallel to μ_{01} (which is realistic for symmetrical molecules), the equation for δ_{2PA} at the excitation laser frequency ν_p, can be written as follows:[38]

$$\delta_{2PA}(E_p) = \frac{32\pi^3}{5c^2h} \frac{E_p^2}{(E_{01} - E_p)^2 + \Gamma_{01}^2} \times$$
$$\left[\frac{|\mu_{01}|^2 |\Delta\mu|^2 \Gamma_{0f1}}{(E_{0f1} - 2E_p)^2 + \Gamma_{0f1}^2} + \frac{|\mu_{01}|^2 |\mu_{1f2}|^2 \Gamma_{0f2}}{(E_{0f2} - 2E_p)^2 + \Gamma_{0f2}^2} + \right.$$
$$\left. \frac{|\mu_{01}|^2 |\mu_{1f3}|^2 \Gamma_{0f3}}{(E_{0f3} - 2E_p)^2 + \Gamma_{0f3}^2} \right] \quad (4)$$

where c is the speed of light, h is Planck's constant, $E_p = h\nu_p$, $E_{01} = h\nu_{01}$, $E_{0f1} = h\nu_{f1}$, $E_{0f2} = h\nu_{f2}$, and $E_{0f3} = h\nu_{f3}$ are the corresponding transition energies and Γ is a damping constant ($\Gamma_{01} = \Gamma_{0f1} = 0.04–0.05$ eV, $\Gamma_{0f2} = \Gamma_{0f3} = 0.1$ eV). The fitting parameters are: $|\Delta\mu|$, $|\mu_{1f2}|$, and $|\mu_{1f3}|$. The results of fitting are shown in Figure 3 by the solid curve and correspond to the best fit values: $\Delta\mu = 3.8$ D, $\mu_{1f2} = 11$ D, and $\mu_{1f3} = 4.6$ D (values for G37 only). From our quantum-chemical calculations, the $S_1 \rightarrow S_2$ transition dipole moment, $\mu_{1f2} = 10$ D, which agrees well with the fitting value and considerably exceeds the typical values (1–2 D) for excited-state transition dipole moment for

cationic polymethines with the same conjugation length.[7] Calculation of μ_{1f} is much more complicated due to a mixing of several transitions, which are involved in the 2PA process. From the above analysis we conclude that the extremely large δ_{2PA} values for this anionic series can be explained by the combination of the large transition dipole moments $\mu_{01} = 13-19$ D and $\mu_{1f} = 9-13$ D. Existence of strong donor diethylamino-groups at the end of the terminal groups allows us to suppose that the molecular structure of the investigated series of dyes has a quadrupolar-like character and can be presented as D-A-π-A-D, rather than A-π-A. This may explain the large excited-state dipole moments as effective charge transfer processes over large distances (for example, from HOMO−1 to HOMO as shown for G37 in Figure 5) resulting in the large 2PA cross-section values (up to ≈17 000 GM).

Quantum-chemical calculations and molecular orbital analysis allow estimation of the positions of the ESA bands, their orientation relative to the $S_0 \rightarrow S_1$ transition, and the nature of MOs responsible for the ESA cross sections. These ESA transitions can be roughly calculated as the energy difference between the positions of the 2PA peaks and the main linear absorption peak assuming that there are no essential changes in the excited-state molecular geometry upon excitation. This is a reasonable assumption for symmetrical cyanine-like molecules with small Stokes shifts, mirror symmetry of absorption and fluorescence spectra, and small solvatochromic effects. More detailed analysis of 2PA and ESA links may be found in our previous publication for polymethine, squaraine and tetraone near-IR molecules.[8]

ESA spectra for all the anionic molecules represent broad bands in the visible range (400−600 nm for G37, 400−630 nm for G38, 450−630 nm for G74, and 450−700 nm for G152) as shown in Figure 4. We observe that the lengthening of the conjugation chain leads to a ≈30−40 nm red shift of the ESA peaks; this red shift is much smaller than for the linear absorption bands. Another experimental feature is connected with the redistribution of the ESA magnitude from the shorter to the longer wavelength band, clearly observed for G152. According to our calculations, for all anionic dyes in the visible spectral range, there are two allowed ESA bands of $1B_1 \rightarrow nA_1$ symmetry. For G37, their calculated positions are 450 and 508 nm, in good agreement with the experimentally measured peaks at 460 and 530 nm. These ESA bands presumably correspond to the $S_1 \rightarrow S_{10}$ and $S_1 \rightarrow S_{12}$ transitions and are connected with the mixture of HOMO-3 → HOMO (smaller contribution) and LUMO → LUMO+2 (larger contribution) transitions. Quantum-chemical calculations of ESA spectra for molecules with longer conjugated chains are more complicated due to more mixing of the excited-state transitions involving a larger number of MOs. From our theoretical findings, ESA bands for G38, G74, and G152 are connected with the $S_1 \rightarrow S_8$ and $S_1 \rightarrow S_{10}$ transitions and their nature is similar to G37 primarily involving the mixture of the same transitions: HOMO−3 → HOMO and LUMO → LUMO+2.

4. Conclusion

We describe a detailed experimental investigation of the linear and nonlinear optical absorption properties of a new series of anionic symmetrical A-π-A polymethine dyes, which contain diethylamino-coumarin-dioxaborine acceptor terminal groups and differ by the length of the conjugated chromophore, from $n = 1$ to $n = 4$. We also perform quantum-chemical analysis that provides insight into the nature of the linear and nonlinear optical processes. The measurements are performed with femto-

and picosecond laser pulseswidths in order to gain an understanding of the intramolecular processes and to obtain unambiguous molecular parameters. These experiments allow for a more complete comparison with modeling of the molecular dynamics. Experimental and quantum-chemical analyses allow us to make the following conclusions:

(1) Polarity of the solvent does not significantly affect the positions of the absorption-fluorescence spectra and the magnitudes of the fluorescence quantum yields for symmetrical anionic A-π-A dyes. In contrast to typical cationic D-π-D series, diethylamino-coumarin-dioxaborine dyes are highly fluorescent in the near-IR range with quantum yields from ≈90% at 640 nm to ≈18% at 840 nm. These large quantum yields in the red to near-IR are important for fluorescence sensing and bioimaging applications.[39]

(2) Excitation anisotropy spectra for all molecules reveal a large alternation of maximum and minimum features (anisotropy ranges from −0.05 to 0.35), confirming that these molecules can be characterized by one-photon allowed and symmetry-forbidden transitions. Anisotropy minima correspond to one-photon forbidden transitions $S_0 \rightarrow S_n$ forming ≈50−60° angles with the direction of the $S_0 \rightarrow S_1$ transition dipole moment and suggest the positions of the final states in the 2PA spectra. Comparison between the positions of 2PA bands, found from femtosecond degenerate measurements and estimated from anisotropy results, verified that excitation anisotropy curves may serve as a guide to indicate the peaks of 2PA bands.

(3) 2PA spectra for all dyes consist of two well-separated bands (for G37 we also observed the third 2PA band). The first 2PA band occurs at an energy shifted to the "blue" range by ≈1000−1200 cm^{-1} as compared to the peak of the $S_0 \rightarrow S_1$ transition, which is typical for symmetrical cyanine-like molecules. This band is attributed to the coupling between the first excited electronic state S_1 and its vibrational modes. The 2PA cross sections of this "vibrational coupling" band strongly increases with the lengthening of the chain conjugation, from ≈140 GM at 1120 nm for G37 ($n = 1$) to ≈2200 GM at $\lambda_{2PA} = 1600$ nm for G152 ($n = 4$). Note that the last value of 2200 GM is one of the largest values, measured for single organic molecules within the telecommunication window (1300−1600 nm).

(4) The position of the second and strongest 2PA band for all anionic molecules corresponds to the S_2 final state that is supported by quantum-chemical calculations and excitation anisotropy measurements. Similar to the first 2PA band, δ_{2PA} values for the second 2PA band increase with the lengthening of the chain from ≈2900 GM at $\lambda_{2PA} = 880$ nm for G37 to ≈17 000 GM at $\lambda_{2PA} = 1100$ nm for G152. The strong donor diethylamino- groups at the end of the terminal groups leads us to suppose that this series of dyes appear to be quadrupolar-like, D-A-π-A-D molecular structures. Large δ_{2PA} values, up to 17 000 GM, are explained by the combination of the large ground to excited-state transition dipole moments, $\mu_{01} = 13-20$ D, and the dipole moments between excited-states, $\mu_{1f} = 9-13$ D.

Efficient Two-Photon Absorbing Polymethine Dyes

J. Phys. Chem. A, Vol. 114, No. 23, 2010 **6501**

References and Notes

(1) Padilha, L. A.; Fu, J.; Hagan, D. J.; Van Stryland, E. W.; Cesar, C. L.; Barbosa, L. C.; Cruz, C. H. B.; Buso, D.; Martucci, A. *Phys. Rev. B* **2007**, *75*, 075325.

(2) Law, W. C.; Yong, K. T.; Baev, A.; Hu, R.; Prasad, P. N. *Opt. Express* **2009**, *17*, 19041.

(3) He, G. S.; Tan, L. S.; Zheng, Q.; Prasad, P. N. *Chem. Rev.* **2008**, *108*, 1245.

(4) Marder, S. R. *Chem. Commun.* **2006**, *2*, 131.

(5) Pawlicki, M.; Collins, H. A.; Denning, R. G.; Anderson, H. L. *Angew. Chem., Int. Ed.* **2009**, *48*, 3244.

(6) Collins, H. A.; Khurana, M.; Moriyama, E. H.; Mariampillai, A.; Dahlstedt, E.; Balaz, M.; Kuimova, M. K.; Drobizhev, M.; Yang, V. X. D.; Phillips, D.; Rebane, A.; Wilson, B. C.; Anderson, H. L. *Nature Phot.* **2008**, *2*, 420.

(7) Fu, J.; Przhonska, O. V.; Padilha, L. A.; Hagan, D. J.; Van Stryland, E. W.; Bondar, M. V.; Slominsky, Y. L.; Kachkovski, A. D. *J. Optic. Soc. Am., B* **2007**, *24*, 56.

(8) Webster, S.; Fu, J.; Padilha, L. A.; Przhonska, O. V.; Hagan, D. J.; Van Stryland, E. W.; Bondar, M. V.; Slominsky, Y. L.; Kachkovski, A. D. *Chem. Phys.* **2008**, *348*, 143.

(9) Halik, M.; Wenseleers, W.; Grasso, C.; Stellacci, F.; Zojer, E.; Barlow, S.; Brédas, J. L.; Perry, J. W.; Marder, S. R. *Chem. Commun.* **2003**, *13*, 1490.

(10) Hales, J. M.; Zheng, S.; Barlow, S.; Marder, S. R.; Perry, J. W. *J. Am. Chem. Soc.* **2006**, *128*, 11362.

(11) Zojer, E.; Wenseleers, W.; Halik, M.; Grasso, C.; Barlow, S.; Perry, J. W.; Marder, S. R.; Brédas, J. L. *ChemPhysChem* **2004**, *5*, 982.

(12) Charlot, M.; Izard, N.; Mongin, O.; Riehl, D.; Blanchard-Desce, M. *Chem. Phys. Lett.* **2006**, *417*, 297.

(13) Belfield, K. D.; Morales, A. R.; Kang, B. S.; Hales, J. M.; Hagan, D. J.; Van Stryland, E. W.; Chapela, V. M.; Percino, J. *Chem. Mater.* **2004**, *16*, 4634.

(14) Barzoukas, M.; Blanchard-Desce, M. *J. Chem. Phys.* **2000**, *113*, 3951.

(15) Terenziani, F.; D'Avino, G.; Painelli, A. *Chem. Phys. Chem.* **2007**, *8*, 2433.

(16) Geskin, V. M.; Bredas, J. L. *Int. J. Quantum Chem.* **2003**, *91*, 303.

(17) Fu, J.; Przhonska, O. V.; Padilha, L. A.; Hagan, D. J.; Van Stryland, E. W.; Bondar, M. V.; Slominsky, Y. L.; Kachkovski, A. D. *J. Optic. Soc. Am., B* **2007**, *24*, 67.

(18) Chung, S. J.; Zheng, S.; Beverina, L.; Odani, T.; Fu, J.; Padilha, L. A.; Biesso, A.; Hales, J. M.; Zhan, X.; Schmidt, K.; Ye, A.; Zojer, E.; Barlow, S.; Hagan, D. J.; Van Stryland, E. W.; Yi, Y.; Shuai, Z.; Pagani, G. A.; Bredas, J. L.; Perry, J. W.; Marder, S. R. *J. Am. Chem. Soc.* **2006**, *128*, 14444.

(19) Halik, M.; Hartmann, H. *Chem.—Eur. J.* **1999**, *5*, 2511.

(20) Gerasov, A. O.; Shandura, M. P.; Kovtun, Y. P. *Dyes Pigm.* **2008**, *77*, 598.

(21) Lepkowicz, R. S.; Przhonska, O. V.; Hales, J. M.; Fu, J.; Hagan, D. J.; Van Stryland, E. W.; Bondar, M. V.; Slominsky, Y. L.; Kachkovski, A. D. *Chem. Phys.* **2004**, *305*, 259.

(22) Magde, D.; Brannon, J. H.; Cremers, T. L.; Olmsted, J. *J. Phys. Chem.* **1979**, *83*, 696.

(23) Webster, S.; Padilha, L. A.; Hu, H.; Przhonska, O. V.; Hagan, D J.; Van Stryland, E. W.; Bondar, M. V.; Davydenko, I. G.; Slominsky, Y. L.; Kachkovski, A. D. *J. Lumin.* **2008**, *128*, 1927.

(24) Lakowicz, J. R. *Principles of Fluorescence Spectroscopy*; Kluwer Academic/Plenum Publishers: New York, 1999.

(25) Strickler, S. J.; Berg, R. A. *J. Chem. Phys.* **1962**, *37*, 814.

(26) Padilha, L. A.; Webster, S.; Przhonska, O. V.; Hu, H.; Peceli, D.; Rosch, J. L.; Bondar, M. V.; Gerasov, A. O.; Kovtun, Y. P.; Shandura, M. P.; Kachkovski, A. D.; Hagan, D. J.; Van Stryland, E. W. *J. Mater. Chem.* **2009**, *40*, 7503.

(27) Negres, R. A.; Przhonska, O. V.; Hagan, D. J.; Van Stryland, E. W.; Bondar, M. V.; Slominsky, Y. L.; Kachkovski, A. D. *IEEE J. Quantum Electron.* **2001**, *7*, 849.

(28) Padilha, L. A.; Webster, S.; Hu, H.; Przhonska, O. V.; Hagan, D. J.; Van Stryland, E. W.; Bondar, M. V.; Davydenko, I. G.; Slominsky, Y. L.; Kachkovski, A. D. *Chem. Phys.* **2008**, *352*, 97.

(29) Sheik-Bahae, M.; Said, A. A.; Hagan, D. J.; Van Stryland, E. W. *IEEE J. Quantum Electron.* **1990**, *26*, 760.

(30) Lepkowicz, R. S.; Cirloganu, C. M.; Fu, J.; Przhonska, O. V.; Hagan, D. J.; Van Stryland, E. W.; Bondar, M. V.; Slominsky, Y. L.; Kachkovski, A. D. *J. Optic. Soc. Am., B* **2005**, *22*, 2664.

(31) Xu, C.; Webb, W. W. *J. Optic. Soc. Am., B* **1996**, *13*, 481.

(32) Signorini, R.; Ferrante, C.; Pedron, D.; Zerbetto, M.; Cecchetto, E.; Slaviero, M.; Fortunati, I.; Collini, E.; Bozio, R.; Abbotto, A.; Beverina, L.; Pagani, G. A. *J. Phys. Chem. A* **2008**, *112*, 4224.

(33) Gerasov, A. O.; Shandura, M. P.; Kovtun, Y. P.; Kachkovsky, A. D. *J. Phys. Org. Chem.* **2008**, *21*, 419.

(34) Scherer, D.; Dorfler, R.; Feldner, A.; Vogtmann, T.; Schwoerer, M.; Lawrentz, U.; Grahn, W.; Lambert, C. *Chem. Phys.* **2002**, *279*, 179.

(35) Painelli, A.; Del Freo, L.; Terenziani, F. *Chem. Phys. Lett.* **2001**, *346*, 470.

(36) Beverina, L.; Fu, J.; Leclercq, A.; Zojer, E.; Pacher, P.; Barlow, S.; Van Stryland, E. W.; Hagan, D. J.; Bredas, J. L.; Marder, S. R. *J. Am. Chem. Soc.* **2005**, *127*, 7282.

(37) Matichak, J. D.; Hales, J. M.; Ohira, S.; Barlow, S.; Jang, S.; Jen, A. K.; Brédas, J.; Perry, J. W.; Marder, S. R. *ChemPhysChem* **2010**, *11*, 130.

(38) Kamada, K.; Ohta, K.; Iwase, Y.; Kondo, K. *Chem. Phys. Lett.* **2003**, *372*, 386.

(39) Li, K.; Feng, S. S.; Wu, A. W.; Pu, K. Y.; Liu, Y.; Liu, B. *Adv. Funct. Mater.* **2009**, *19*, 3535.